Seismic analysis for fractured reservoirs of South Komie 3D data

Khaled Al Dulaijan and Gary F. Margrave

ABSTRACT

The South Komie 3D seismic data was acquired within the Horn River basin of northeast British Columbia. The Horn River basin has two main targets of shale gas: the Muskwa and Evie formations. Even though being an unconventional reservoir, standard seismic techniques are quite useful for such reservoirs. South Komie 3D seismic data is analyzed to identify gas sweet spots. Because the reservoirs consist of shale. Fractures are important because they can act as fluid conduits. There, the data is analyzed to identify fractures as well.

In this study, a strong channel system is observed within the near surface. The post-stack P-impedance inversion can help indicating sweet spots within Evie and Muskawa reservoirs. Also, post-stack amplitude, instantaneous frequency, and curvature attributes are useful for identifying fracture direction and intensity. Results of amplitude and instantaneous frequency correlate very well with in Evie reservoir. AVO analysis was found to help identifying top and base of Evie gas away from the well.

INTRODUCTION

Standard geophysical workflows continue to play a key role for the development of unconventional reservoirs. Those workflows help mapping geological horizons and major faults, identifying seismic-rock relations, and finding sweet spots. For shale gas reservoirs in the Horn rivers basin, we have utilized standard geophysical techniques, such as seismic imaging, post-stack seismic inversion and attributes, and AVO analysis. In such reservoirs, the seismic role can be extended to azimuthal analysis of amplitude and velocity, converted PS data processing, and 4D seismic.

In this paper, shale gas reservoirs, in the Horn River basin, are studied using standard geophysical techniques. Our analysis includes post-stack impedance inversion, post-stack seismic attributes, and amplitude variation with offset (AVO).

THE HORN RIVER BASIN

The Horn River Basin is located mainly in northeast British Columbia (BC), and partially in the southwest Northern Territories (NT), Canada. The Horn River Basin is separated by carbonate reef from the Cordova Basin to the east and separated by the Bovie Fault from the Liard Basin to the west. It extends to an area of 18,000 km^2 (Advanced Resources International, 2013) and has 200 producing wells as of February 2014. Estimated original gas in place (OGIP) is 500 Tcf (Adams, 2014)). The Horn River basin is indicated by red in Figure 1. Figure 2 shows an east-west stratigraphic cross

section where Liard Basin, Bovie fault, Horn River Basin, Keg River carbonate reef, and Cordova Basin can be seen when going from west to east. Main targets are the Devonian shale of Muskawa and Evie. Muskawa is below the Fort Simpson and above the Otter Park. The Otter Park consists of shale in the upper part and clay in the lower part, followed by Evie Shale. Figure 3 shows the stratigraphic column of Horn River Basin.
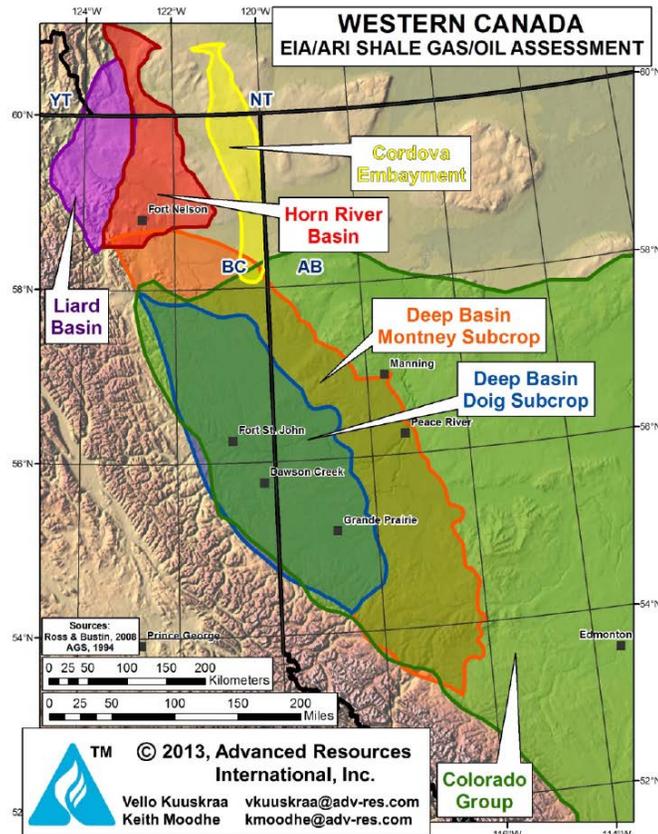
Fig. 1. Horn River Basin is located in mainly in northeast BC and partially in southwest NT. It is indicated by the red color between the Liard Basin (purple) and the Cordova basin (yellow). Its area is about 18,000 km² (after Advanced Resources International Inc, 2013)
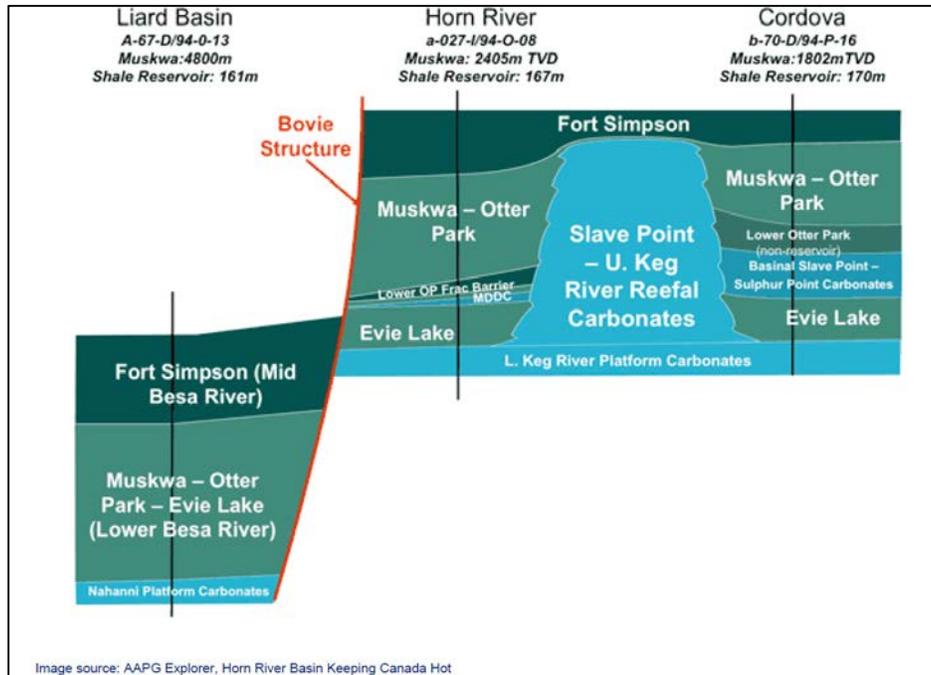
Fig. 2. An east-west stratigraphic cross section. From west to east, Liard Basin, Bovie fault, Horn River Basin, Keg River carbonate reef, and Cordova Basin are show (after McGowen).
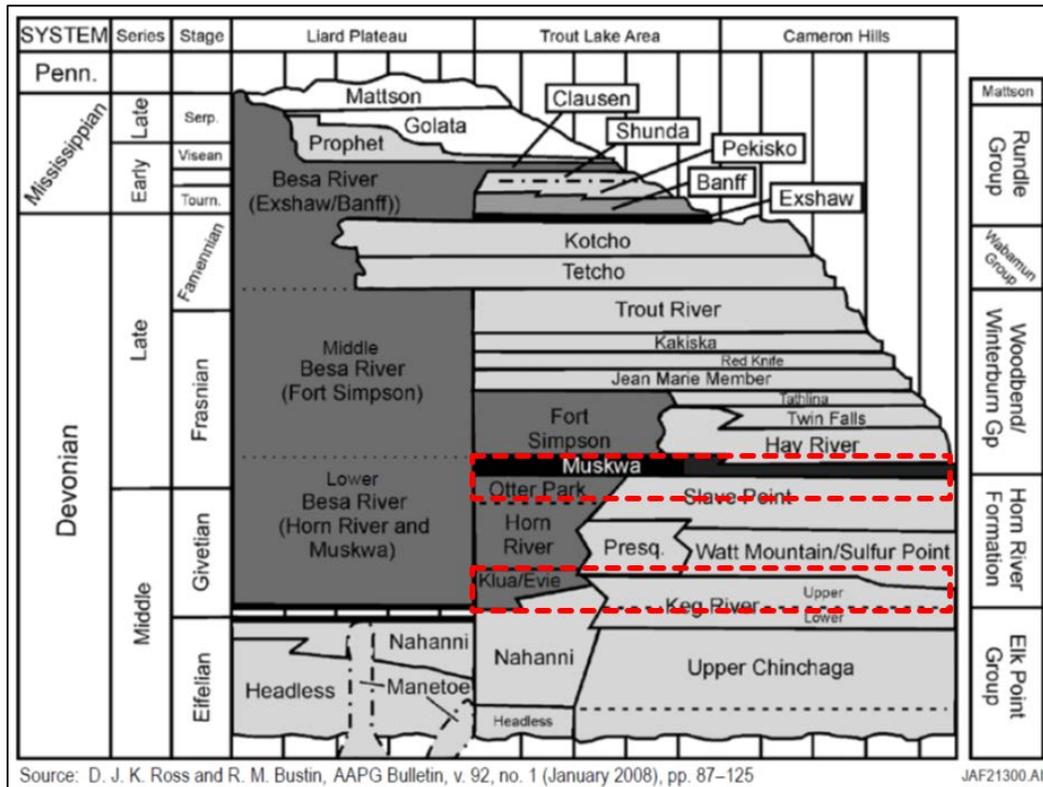
Fig. 3. Stratigraphy of the Horn River Basins. Main targets are Devonian Muskawa and Evie shale. Muskawa is below Fort Simpson and Otter Park. Otter Park consists of shale in the upper part and clay in the lower part, followed by Evie Shale (After Ross and Bustin, 2008).

SEISMIC DATA ACQUISTION AND PROCESSING

South Komie 3D data was acquired in the central Horn River Basin. The Data was acquired by Geokinetics, in March 2009. Each source was 2 kilograms of dynamite buried at depth of 15 m. For the receivers, single 3-C geophones were used. The source and the receiver intervals are 60 m, with source lines oriented in the north-south direction and receiver lines oriented at east-west direction. Source line and receiver line spacings are 360 m and 240 m respectively. The record length was 10 seconds with a sample rate of 2 ms.

South Komie PP and PS data were processed by Sensor Geophysical Limited. The processing workflow consists of SEGY input, geometry assignment, killing bad traces, surface-consistent amplitude scaling, offset amplitude recovery, and followed by statics. For statics, a 2-layer model obtained by refraction was used. The second refactor is shown in Figure 4. A significant channel system within the near surface is observed. Linear noise attenuation, FK filter, surface-consistent deconvolution and amplitude scaling were applied. VTI NMO was applied after testing different eta values (reference to Thomsen's paper). The values that were tested were 0.1, 0.12, and 0.14. Test results are shown in Figure 5. A hockey stick effect can be seen at large offsets around 700 ms and 1400 ms. Muskwa reservoir is around 1400 ms. The VTI anisotropic effect is minimal on the gather that has eta of 0.12. Therefore, a constant eta of 12% were applied to the data. Data was binned as common-offset vector (COV) tiles (can we reference something here about COV??) to preserve azimuthal variations prior to PSTM. Kirchoff 3D PSTM was applied, and followed by an outer mute. PSTM gathers with mute function are shown in Figure 6. The reflection energy looks reasonably flat on the PSTM gather, but the mute seems harsh.
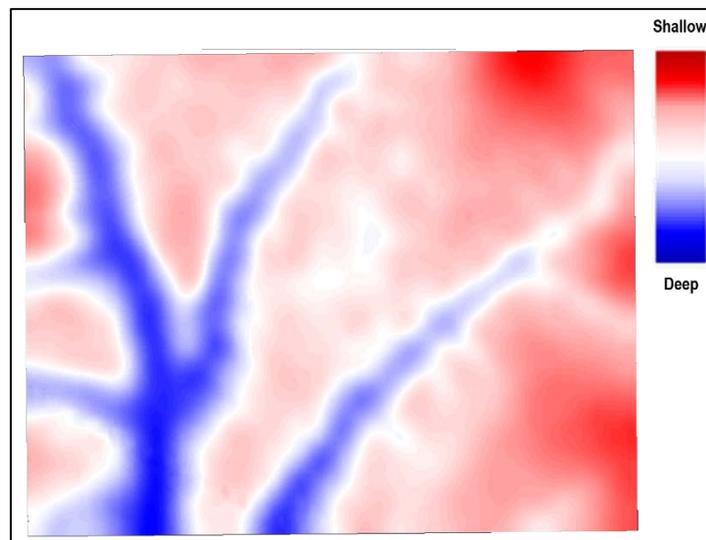
Fig. 4. Second refractor elevations. Blue is deep and red is shallow. A significant channel system within the near surface is observed.
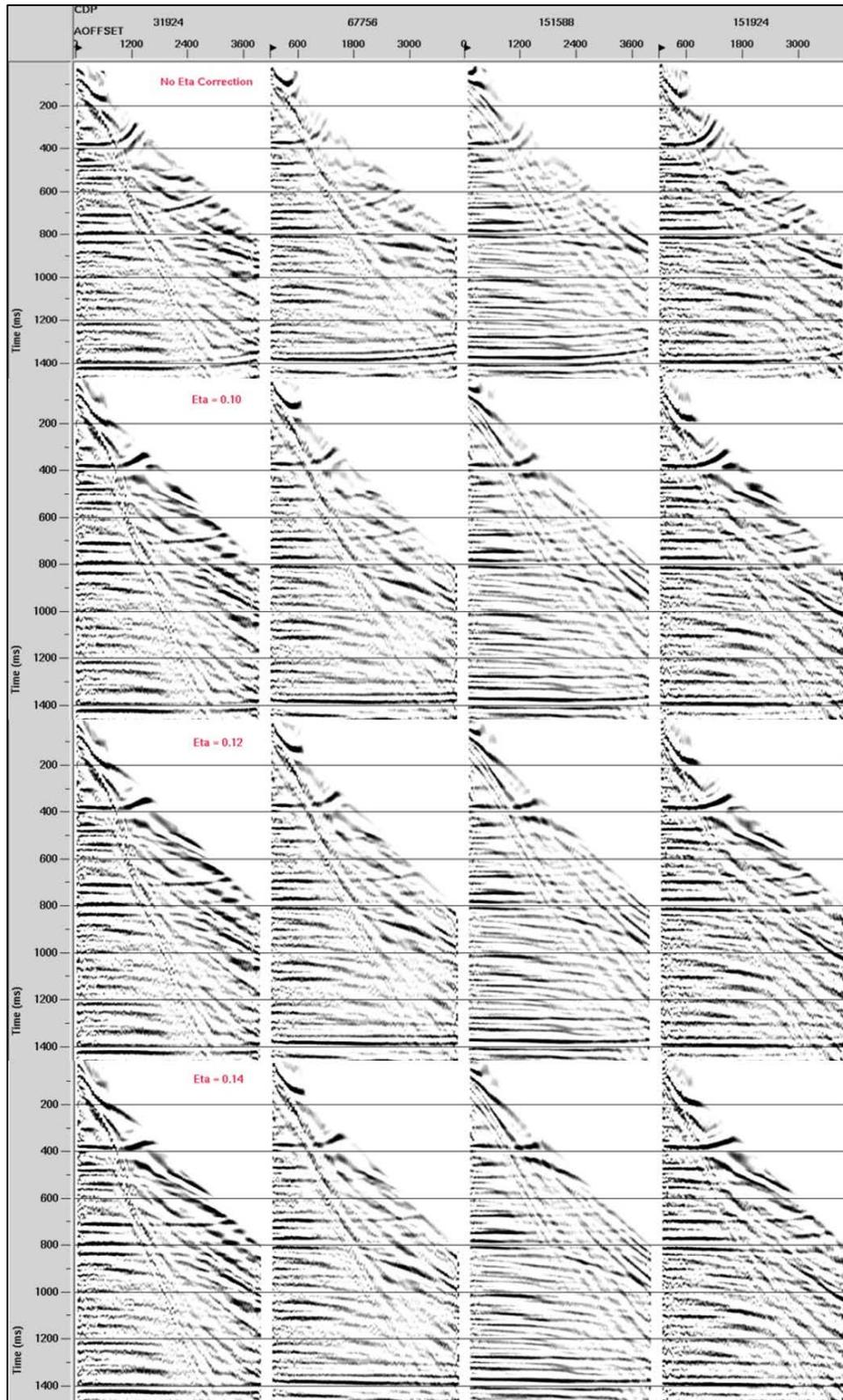
Fig. 5. CDP Gathers with different Eta values. From the top to the bottom, eta values are null, 0.1, 0.12, and 0.14. The CDP gathers with no eta applied show clearly the hockey stick effect

(anisotropy) at the far offset around 700 ms and 1400 ms. Anisotropic effect is least on the gather that has eta of 0.12.
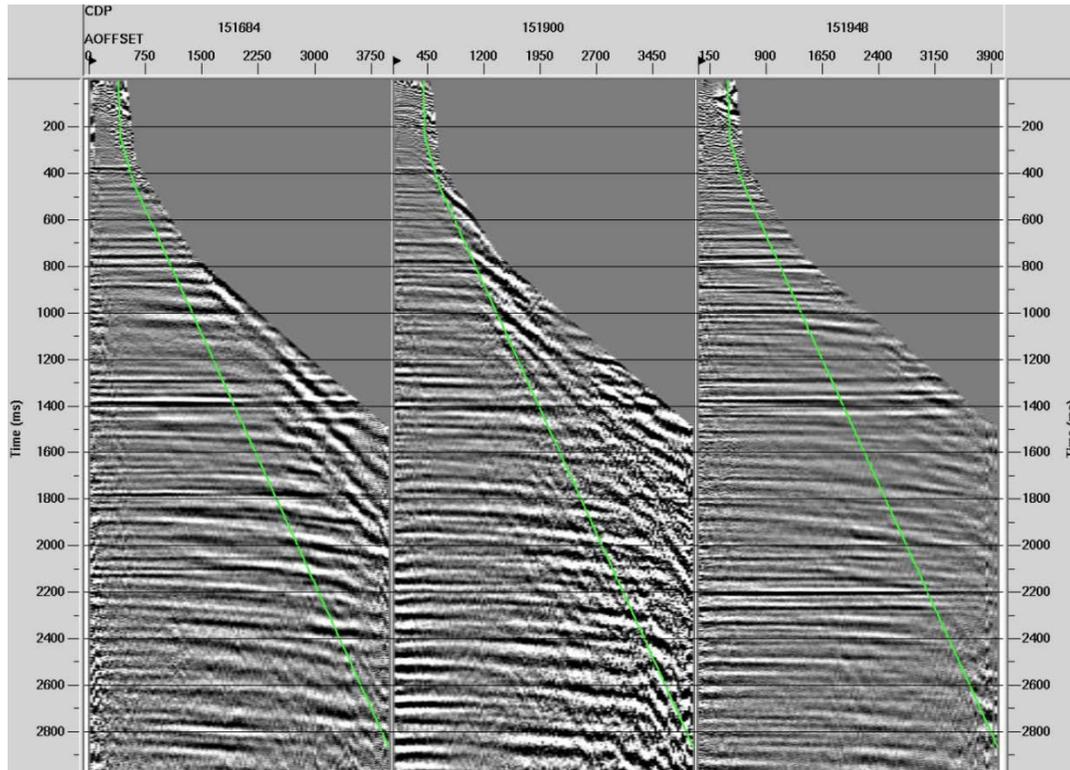
Fig. 6. PSTM image gathers with an outer mute function indicated by green.

POST-STACK P-IMPEDANCE INVERSION

The first analysis step is correlating the surface seismic data to a synthetic seismimogram computed from well logs. This step is very important because of many important outcomes (i.e. wavelet used for inversion, depth-time relation, and horizon picks). From the sonic and density logs, the P-impedance is derived, and therefore used to calculate reflection coefficients. If the reflection coefficients are known at the well in the seismic data, we can accurately estimate the wavelet and then take it out of the data. Within the south Komie 3D, well logs of two wells are available. Those two wells were used to extract a single wavelet.

Figure 7 shows well log calibration with surface seismic data. Surface seismic data are indicated by black wiggles. Four well tops are shown: Muskwa, Otter Park, Evie, and Keg River. Corresponding horizons are picked and shown in the surface seismic section. The density log is indicated by blue and the P-wave velocity calculated from sonic log is indicated by light green. From those two logs, P-wave impedance is calculated, shown by the dark green log, and used beside the extracted wavelet to calculate the synthetic seismogram(blue wiggles). Correlation between synthetic (blue) and real seismic (red) is about 70% for both wells. S-wave velocity log calculated from S-wave sonic is shown by red, Vp/Vs ratio log is calculated and shown by magenta, and Gamma Ray log is shown

by gray. Both reservoir (Muskwa and Evi) have low Vp/Vs ratio and high gamma ray values. Low Vp/Vs ratio can indicate presence of gas, while high gamma ray values indicate shale. Clean sand has a low Gamma Ray values as shown in the log up to 1400 ms. Below 1400 ms, a sandy shale Gamma Ray log can be seen just above the Muskwa shale.

Tops from well logs were used to pick seismic horizon on 3D PSTM stacked volume. Figure 8 shows a stack across one of the wells with few picked horizons. Muskwa and Evie are indicated by dark red and light blue respectively. Figures 9 and 10 show two-way-time of Muskwa and Evie respectively. Two wells (A-6 & A-9) are within south komie and indicated by both maps. Both maps show dipping toward northeast direction to the Bovie fault.

Post-stack P-impedance inversion analysis, at one well location, is shown by Figure 11. The black curve is the initial P-impedance model obtained by smoothing well data (red). Blue is the P-impedance inversion results. From inverted P-impedance or reflection coefficients a synthetic trace is calculated. Red and black wiggles are inversion and actual seismic respectively. The correlation is more than 0.9 which is excellent. Difference between inversion and actual trace is shown by the wiggles on the right. Inversion was applied to the 3D seismic volume using P-impedance model from two wells. Well data are smoothed, so low frequency model is used as hard data while high frequency from seismic as soft data. Figures 12 and 13 show P-impedance inversion results across the two wells. Computed P-impedance from well logs are inserted. Low P-impedance of Exshaw, Muskwa, and Evie, and high P-impedance of Tetcho and Kaisa prove a good correlation between computed and inverted P-impedance. Low P-impedance can indicate gas.
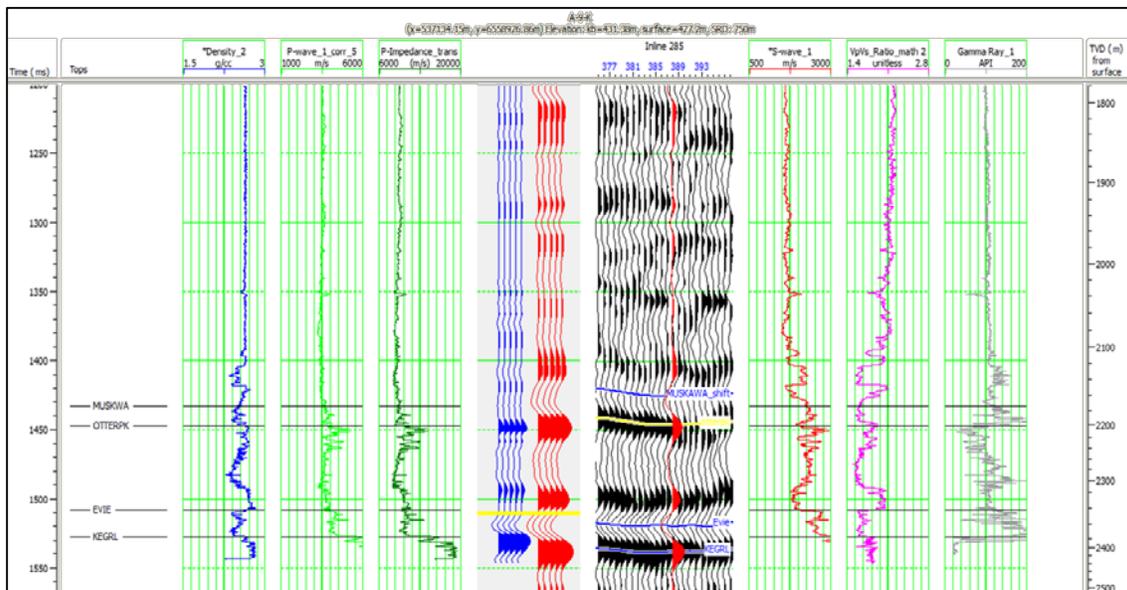
Fig. 7. Well log correlation with surface seismic data. Surface seismic data are indicated by black wiggles. Four well tops are shown: Muskwa, Otter Park, Evie, and Keg River. Corresponding

horizons are picked and shown in the surface seismic section. Density log is indicated by blue and P-wave velocity calculated from sonic log is indicated by light green. From those two logs, P-wave impedance are calculated, shown by the dark green log, and used to calculate synthetic (blue wiggles). Correlation between synthetic (blue) and real seismic (red) is about 70% for both wells. S-wave velocity log calculated from S-wave sonic is shown by red, Vp/Vs ratio log is calculated and shown by magenta, and Gamma Ray log is shown by gray. Both reservoir (Muskwa and Evi) have low Vp/Vs ratio and high gamma ray values
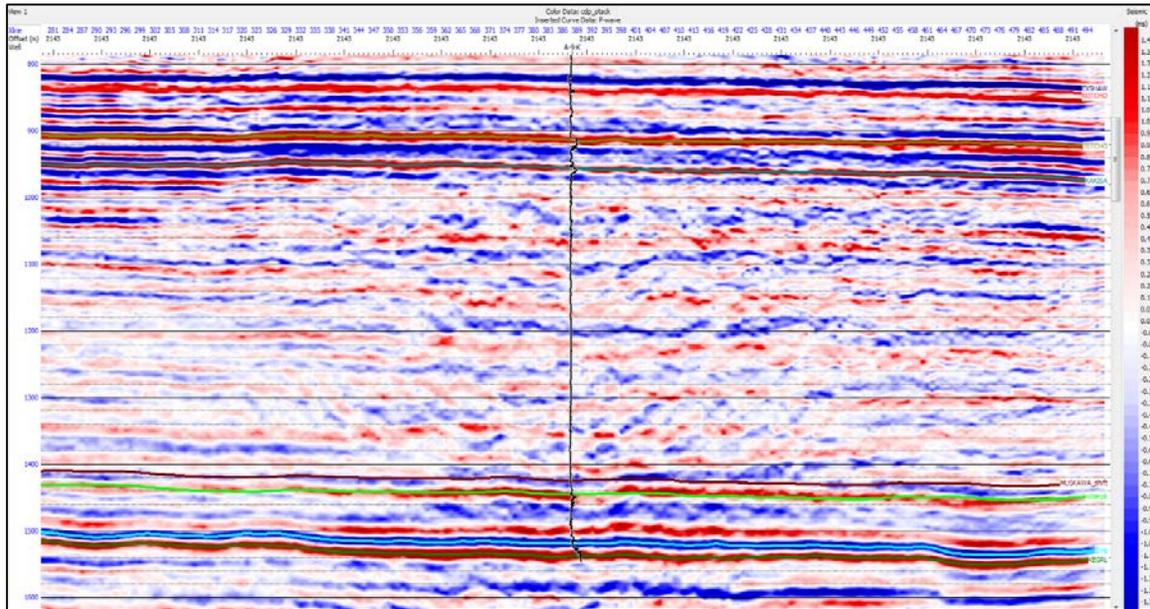
Fig. 8. In-line seismic section showing one well in the middle and 7 picked horizons.
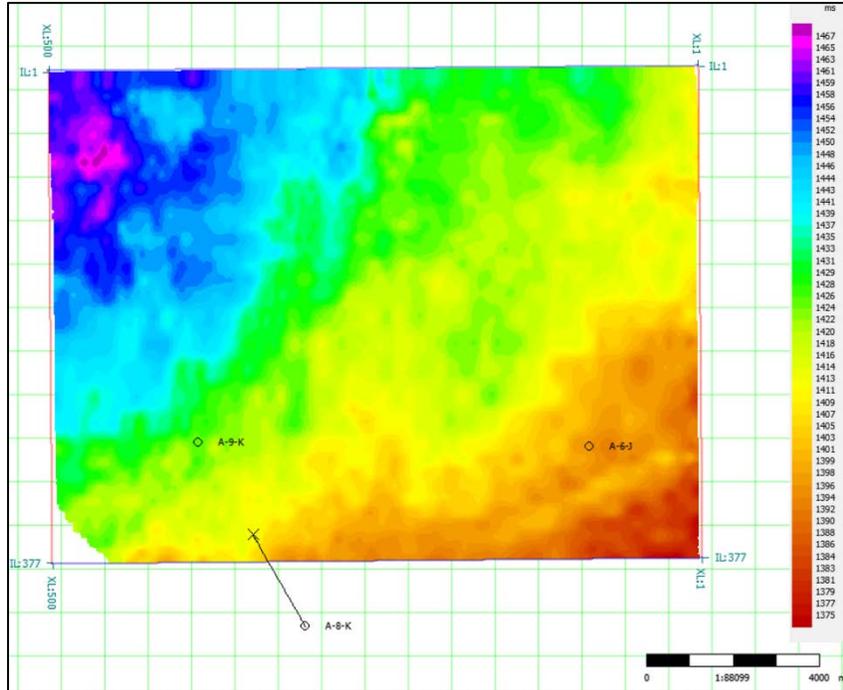
Fig. 9. Muskwa: picked two-way-time in ms.
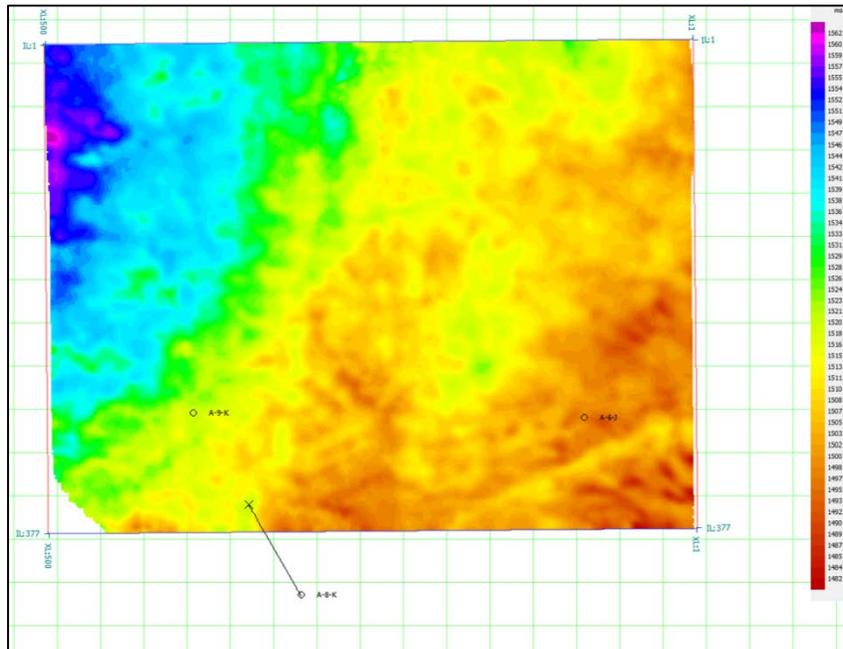
Fig. 10. Evi: picked two-way-time in ms.
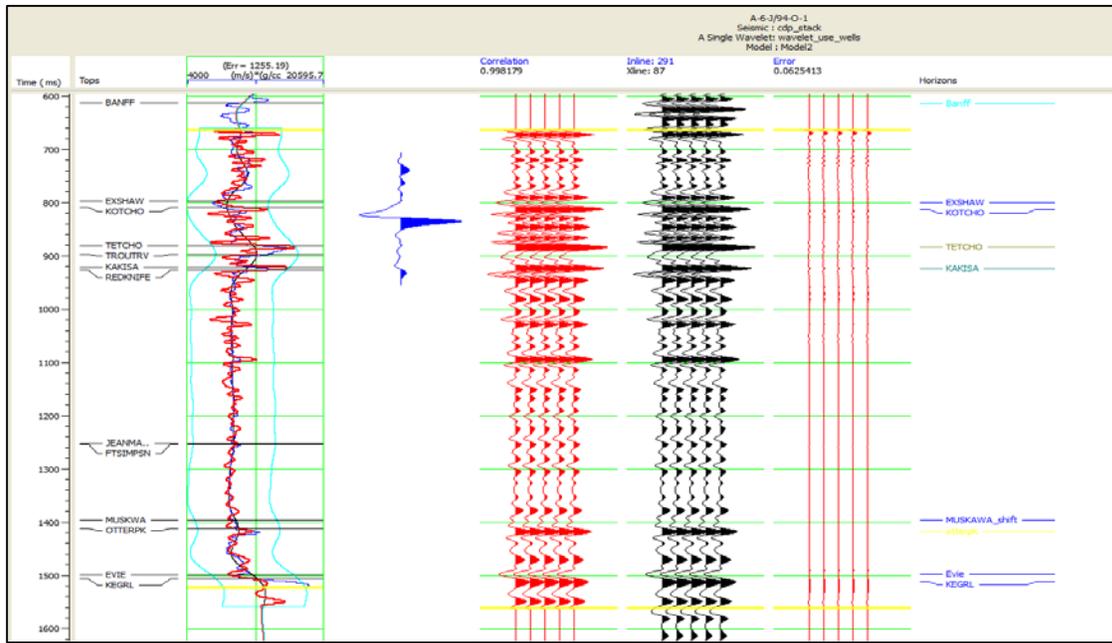
Fig. 11. Post-stack P-impedance inversion analysis at one well location. Black curve is the initial P-impedance model obtained by smoothing well data (red). Blue is the inversion results. Red and black wiggles are inversion and actual seismic respectively. Correlation is more than 0.9.
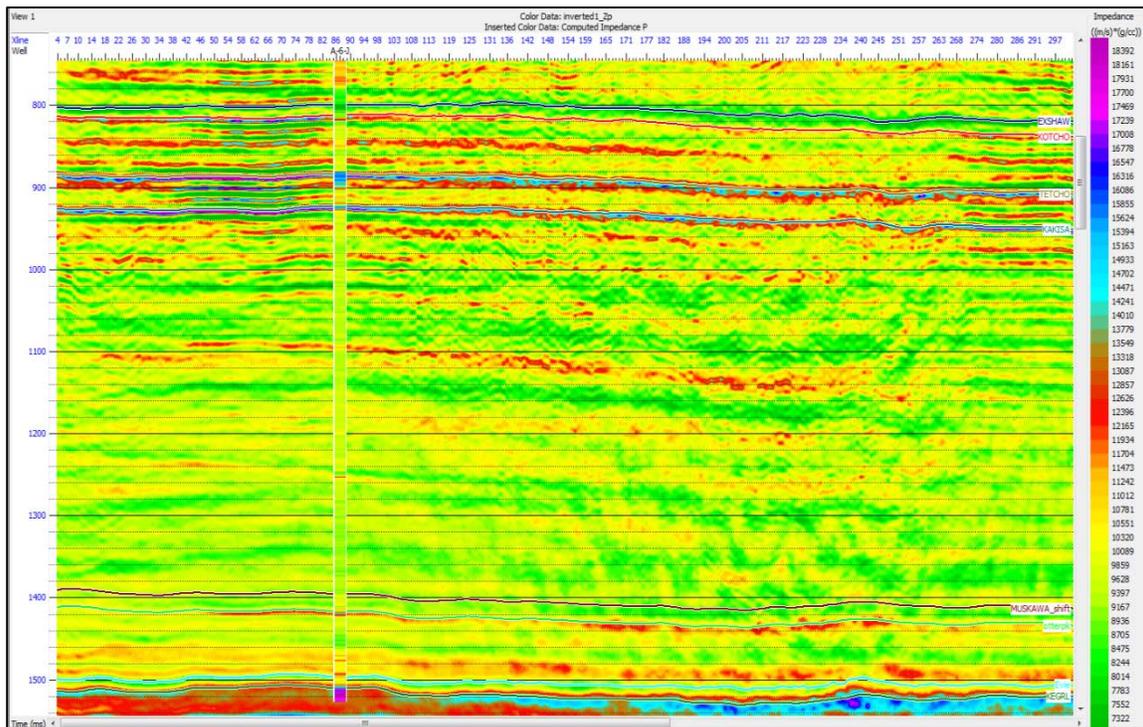
Fig. 12. Post stack P-impedance inversion results. Computed P-impedance from one well is shown at the well location.
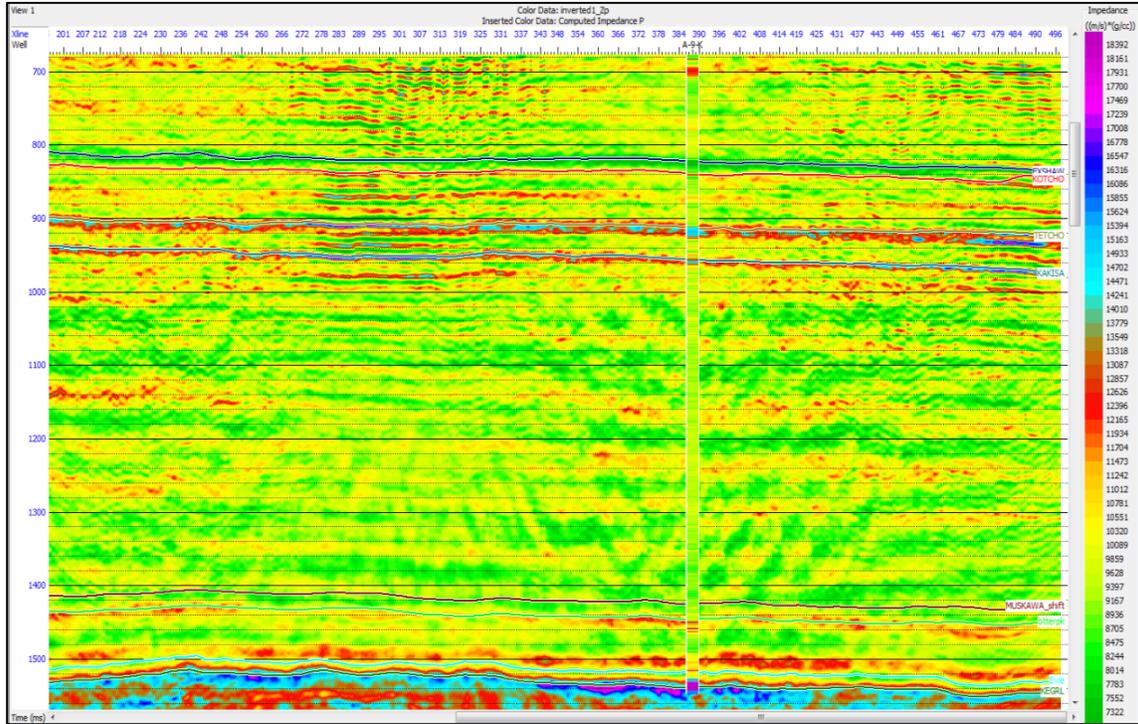
Fig. 13. Post stack P-impedance inversion results. Computed P-impedance from one well is shown at the well location.

POST-STACK SESMIC ATTRIBUTES

Azimuth-limited raw amplitude, instantaneous frequency, and curvature attributes are analyzed here. The PSTM gathers were grouped by azimuth with first group being 0° to 20° and last group being 160° to 180°. The each group is stacked. From each group stacked volume, RMS amplitude was extracted from a window around the Evie horizon. Figure 14 shows azimuth-limited RMS average amplitude at Evie reservoir, with the red arrows indicating azimuths. Black color indicates lower amplitude values, or in another word lower impedance contrast. Therefore, it indicates the direction of fracture strike. Major directions are 0° (i.e. Well A-9) and 90° (i.e. Well A-6).

Instantaneous frequency is calculated from the complex trace, $c(t)$:

$$c(t) = s(t) + i\, h(t) \qquad (1)$$

where $s(t)$ is seismic trace and $h(t)$ is the Hilbert transform of the seismic trace (Taner, 1979). Amplitude envelope, $A(t)$, instantaneous phase, $\emptyset(t)$, and instantaneous frequency, $w(t)$, are calculated by

$$A(t) = \sqrt{s^2(t) + s^2(t)}, \qquad (2)$$

$$\emptyset(t) = tan^{-1}\left(\frac{h(t)}{s(t)}\right), \qquad (3)$$

$$w(t) = \frac{d\emptyset(t)}{dt}. \qquad (4)$$

Instantaneous frequency volume is calculated from post-stack data, using the same azimuth groups used for amplitude analysis. Fig. 15 shows azimuth-limited instantaneous frequency, with black arrows indicating azimuth. Lower instantaneous frequencies see more fractures. Therefore, higher values indicate the fracture strike. Major directions are 0° (i.e. Well A-9) and 90° (i.e. Well A-6). There is a good correlation between amplitude and instantaneous frequency analysis.

The last attribute that was analyzed was the curvature attribute. The amount of bending for a specific point on a horizon defines the curvature k. For example, the surface in Figure 16 shows curvature for the Evie horizon in three dimensions, showing maximum curvature *kmax*, minimum curvature *kmin*, dip curvature *kdip*, and strike curvature *kstr*. Not shown are Gaussian curvature kg, mean curvature *kmean*, most positive curvature *kpos*, and most negative curvature *kneg*. In this case, both maximum and minimum curvatures are positive (Roberts 2001). Figure 17, from left to right, shows the *kmin, kmax,* and *kstr.* Maximum curvature is useful to identify the intensity of fractures and faults (Roberts, 2011). Maximum and minimum curvature correlate very well. The curvature azimuth map indicates that the major trends are about 0° and 40°.
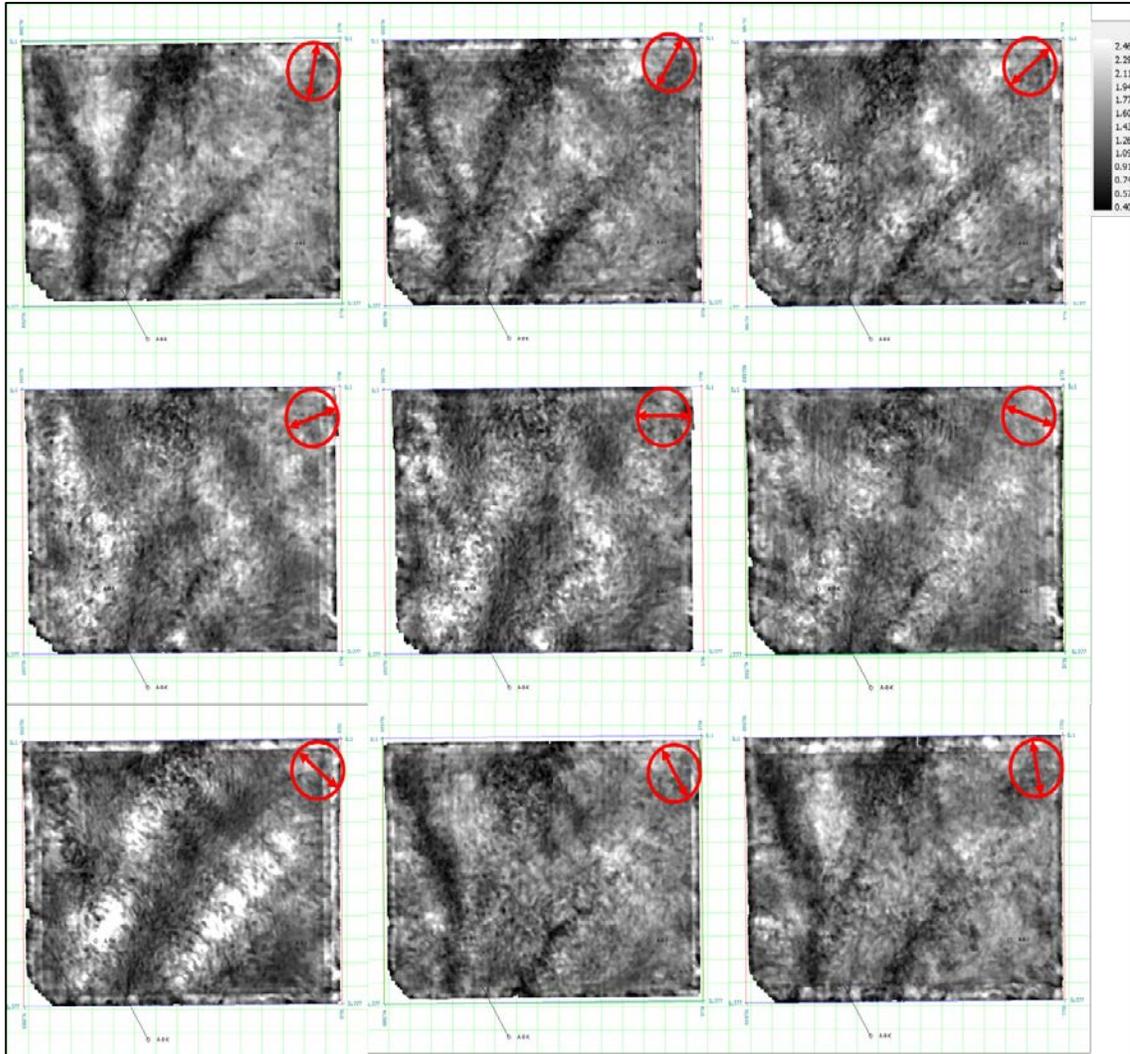
Fig. 14. Azimuth-limited RMS average amplitude at Evie reservoir. Red arrows indicate azimuths. Black indicate lower amplitude values, or in another word lower impedance contrast. Therefore, it indicates the direction of fracture strike. Major directions are 0° (i.e. Well A-9) and 90° (i.e. Well A-6).
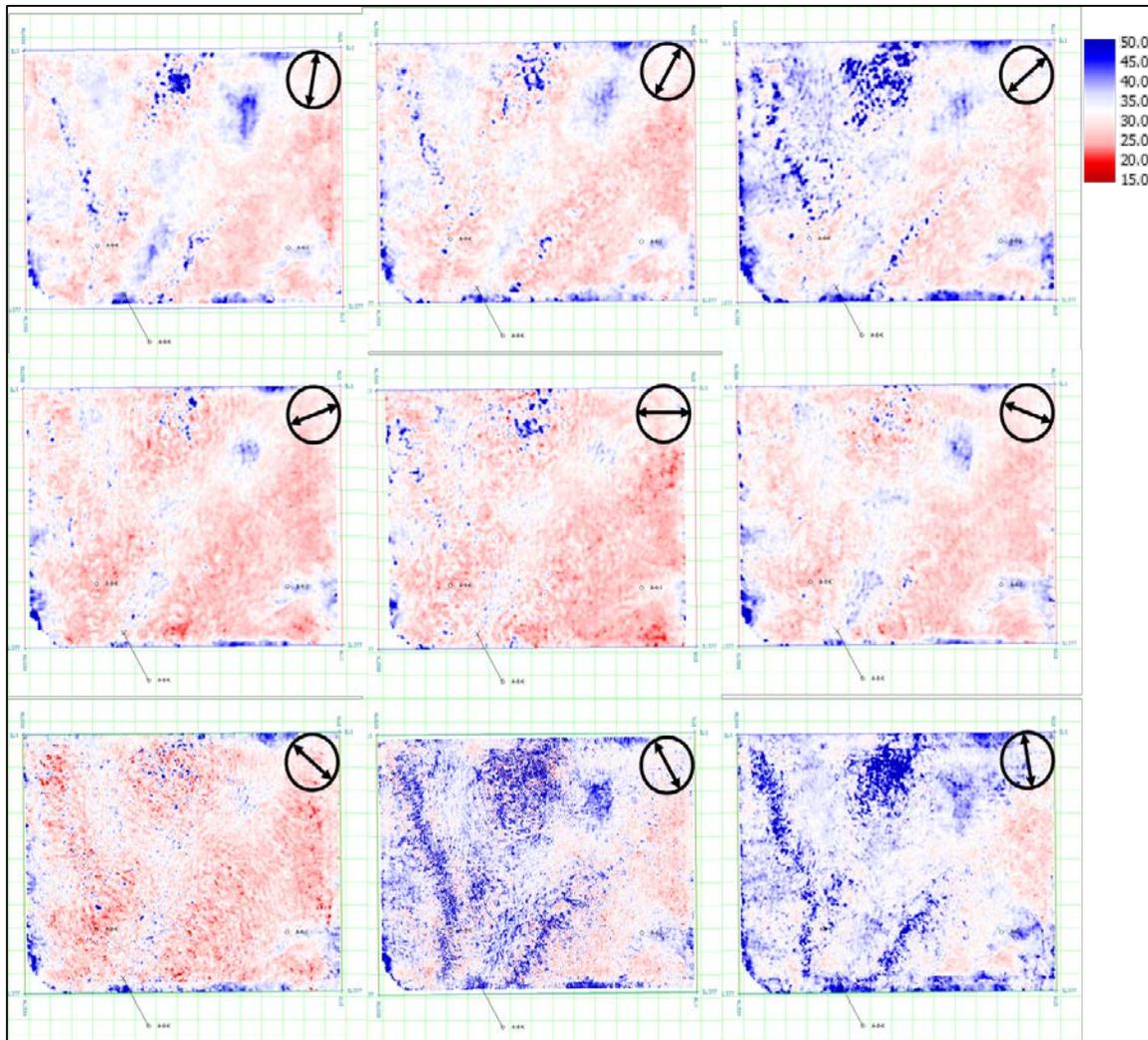
Fig. 15. Azimuth-limited instantaneous frequency. Black Arrows indicate azimuth. Lower instantaneous frequencies see more fractures. Therefore, higher values indicate the fracture strike. Major directions are 0º (i.e. Well A-9) and 90º (i.e. Well A-6).
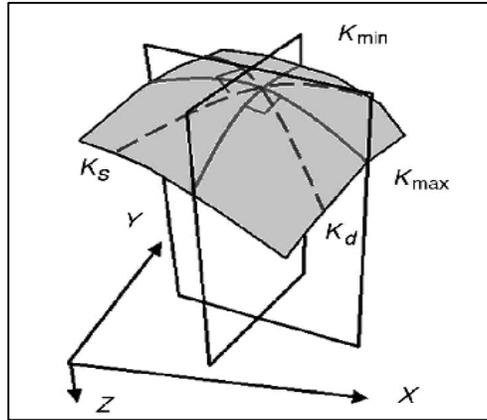
Fig. 16. Curvature in three dimensions, showing maximum curvature ***k*max**, minimum curvature ***k*min**, dip curvature ***k*dip**, and strike curvature ***k*str**. Not shown are Gaussian curvature ***k*g**, mean curvature ***k*mean**, most positive curvature ***k*pos**, and most negative curvature ***k*neg**. In this case, both maximum and minimum curvatures are positive. (After Roberts, 2001)
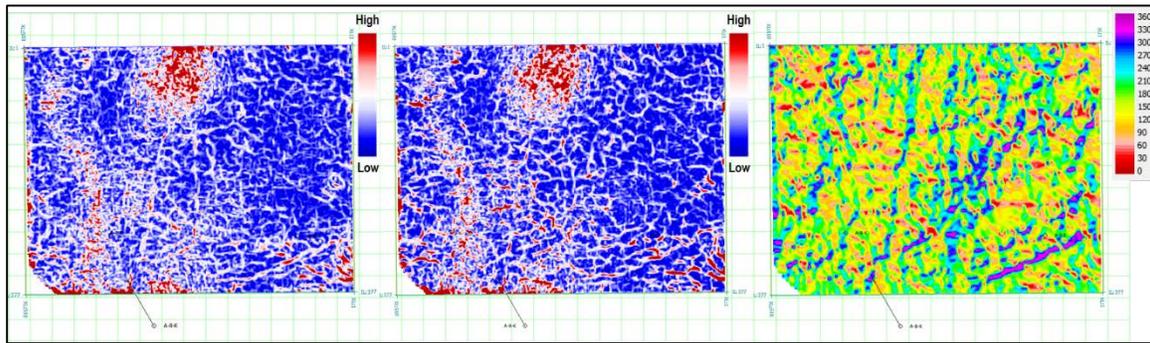
Fig. 17. Curvature attributes of Evie reservoir: Minimum curvature (left), Maximum Curvature (Middle), Azimuth (right). High curvature values indicate fractured zones. Azimuth map indicates that the major trends are about 0º and 40º.

AMPLITUDE VARIATON WITH ANGLE

The reflection and transmission coefficient of non-zero incident angles ($\emptyset$) is given by a sequence of equations known as Zoeppritz equations (Aki and Richards, 2002). We have used a three-term approximation Aki-Richards approximation for P-wave reflection as function of incident angle. The three-term equation is

$$Rpp(\emptyset) = A + Bsin^2\emptyset + Ctan^2\emptyset sin^2\emptyset, \tag{5}$$

where

$$A = \frac{1}{2}\left[\frac{\Delta Vp}{Vp} + \frac{\Delta \rho}{\rho}\right], \tag{6}$$

$$B = \frac{1}{2}\frac{\Delta Vp}{Vp} - 4\left[\frac{Vs}{Vp}\right]^2\frac{\Delta Vs}{Vs} - 2\left[\frac{Vs}{Vp}\right]^2\frac{\Delta \rho}{\rho}, \tag{7}$$

$$B = \frac{1}{2}\frac{\Delta Vp}{Vp}. \tag{8}$$

A, B, and *C* are the intercept, gradient and curvature respectively. ΔVp, ΔVs, and $\Delta \rho$ are the differences in P-wave velocity, S-wave velocity, density of the two media. Vp, s, and ρ are the average P-wave velocity, S-wave velocity, and density of the two media. The advantage of using approximation, such as Aki-Richards, and Schuey is the graphic representation of reflection coefficients (Rüger, 2002).

Using the well logs, reflection coefficients of Evie reservoir top and base are calculated from Aki-Richards. Then, a synthetic angle gather is created and shown in Figure 18 (left). In the middle, the amplitude curve for top of the reservoir is indicated by red, while base of the reservoir is indicated by green. Top of the reservoir has a negative intercept and its amplitude decreases. It has a positive gradient. On the other hand, the base of the reservoir has a positive intercept and its amplitude decreases. It has a negative gradient. That is a characteristic of class IV AVO. 5x5 super gathers are created from PSTM gathers. Figure 19 shows the super gathers around one of the well. Color indicates incident angle and calculated from the ray parameter (p) (CGGVeritas, 2014):

$$p = \frac{\sin e}{Vint} \tag{9}$$

Ray parameter (p) can also be calculated by taking the space (offset), x, derivatives of NMO equation:

$$t_x^2 = t_0^2 + \frac{x^2}{Vrms^2}, \tag{10}$$

$$p = \frac{dt}{dx}, \tag{11}$$

$$\frac{dt}{dx} = \frac{x}{t_x Vrms^2}. \tag{12}$$

Rewriting equation (9) yields

$$\sin e = \frac{x\,Vint}{t_x Vrms^2}. \tag{13}$$

From the geometry of source-receiver pair in a single constant velocity layer shown in Figure 19

$$t_x = \frac{t_0}{\cos e}. \tag{14}$$

For, a single layer $Vint$ and $Vrms$ are equal, therefore substituting equation (14) into equation (13) yields:

$$\tan e = \frac{x}{t_0 Vint}. \tag{15}$$

At target levels, angles can be used up to 29º, as shown by Figure 19. Figure 20 shows angle gathers with amplitude analysis for the top and base of the Evie reservoir. Like the modeled data in Figure 18, the real data shows class IV avo behavior at well A-6. For the other well, AVO was not observed for the Evie reservoir but was observed at nearby locations. A cross plot of intercept and gradient was created for the volume and shown by the bottom of Figure 21. Negative intercept and positive gradient is indicated by red on cross plot and on the above cross section. It represents top of class IV reservoir. Blue repents the bottom of the reservoir. Evie and Keg River are top and base of a class IV reservoir for most of the section.
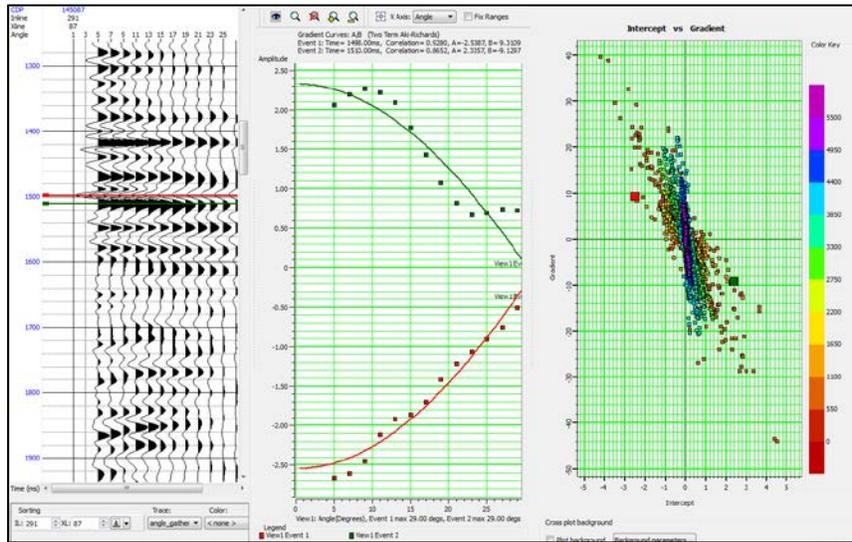
Fig. 18. AVO modelling: synthetic angle gather (left), amplitude curves (middle), and intercept vs. gradient plot (right).
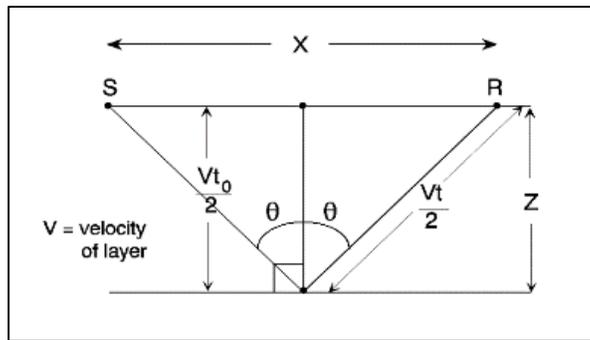
Fig. 19 Raypath of a source-receiver pair in a single constant velocity layer.
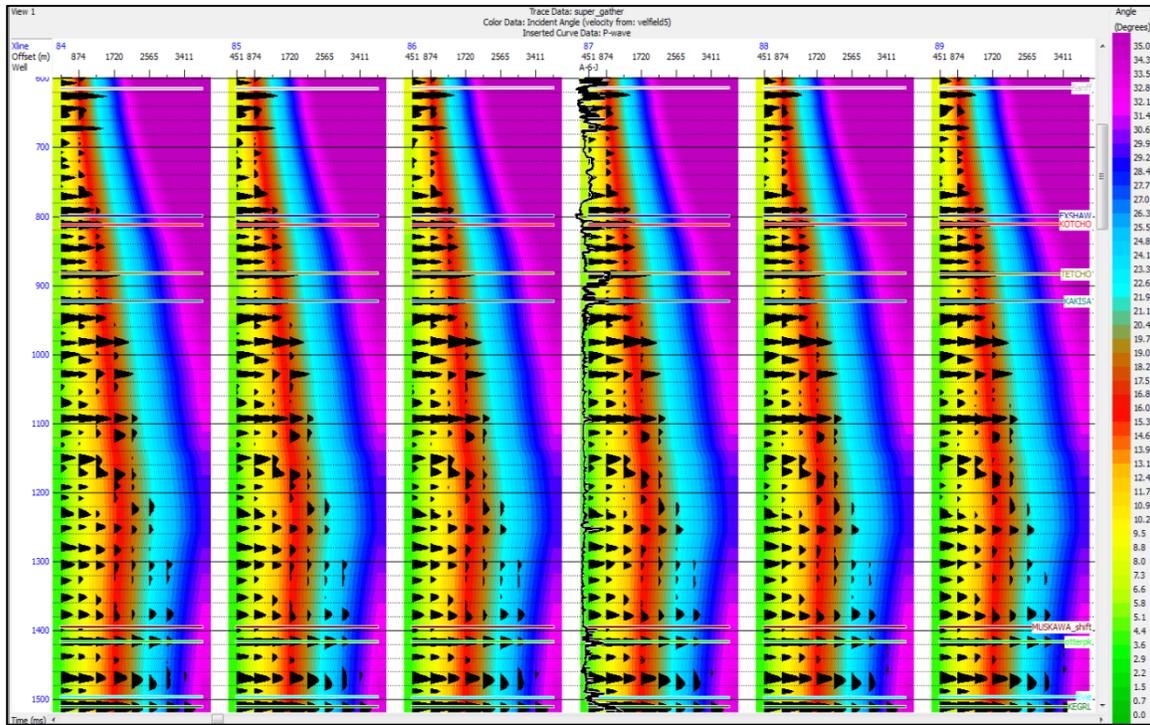
Fig. 19. Supergathers around a well. Color indicate the angle of incident. At target levels, angles can be used up to 29°.
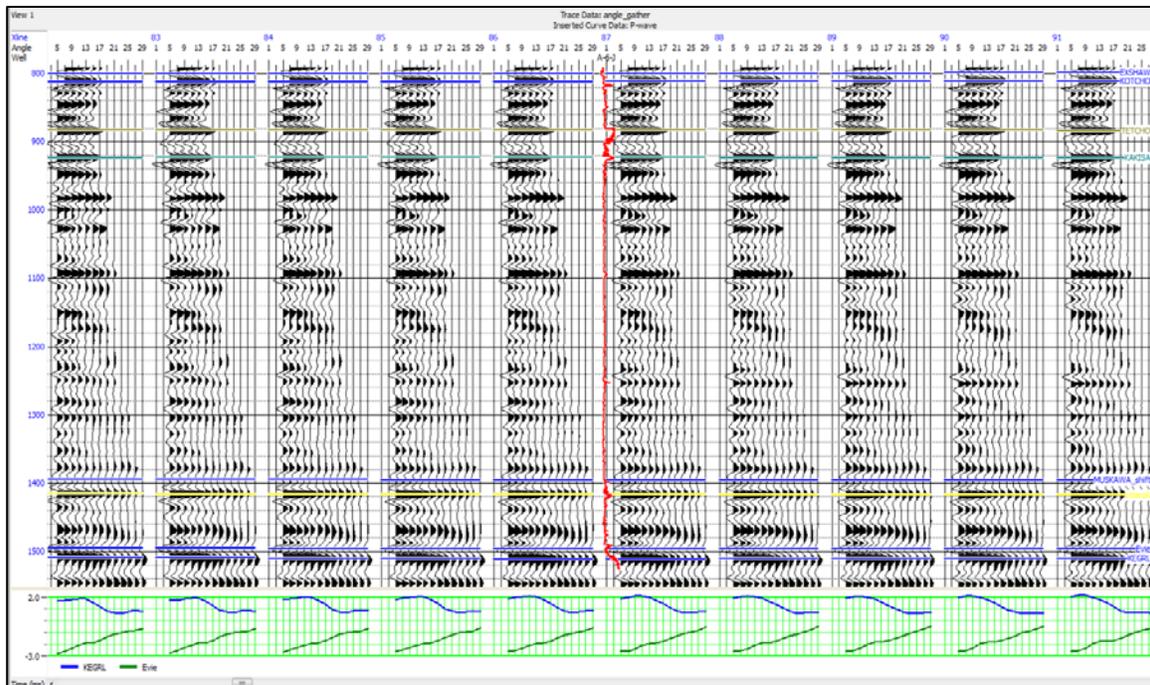
Fig. 20. Angle gathers with amplitude analysis for the top and base of the Evie reservoir.
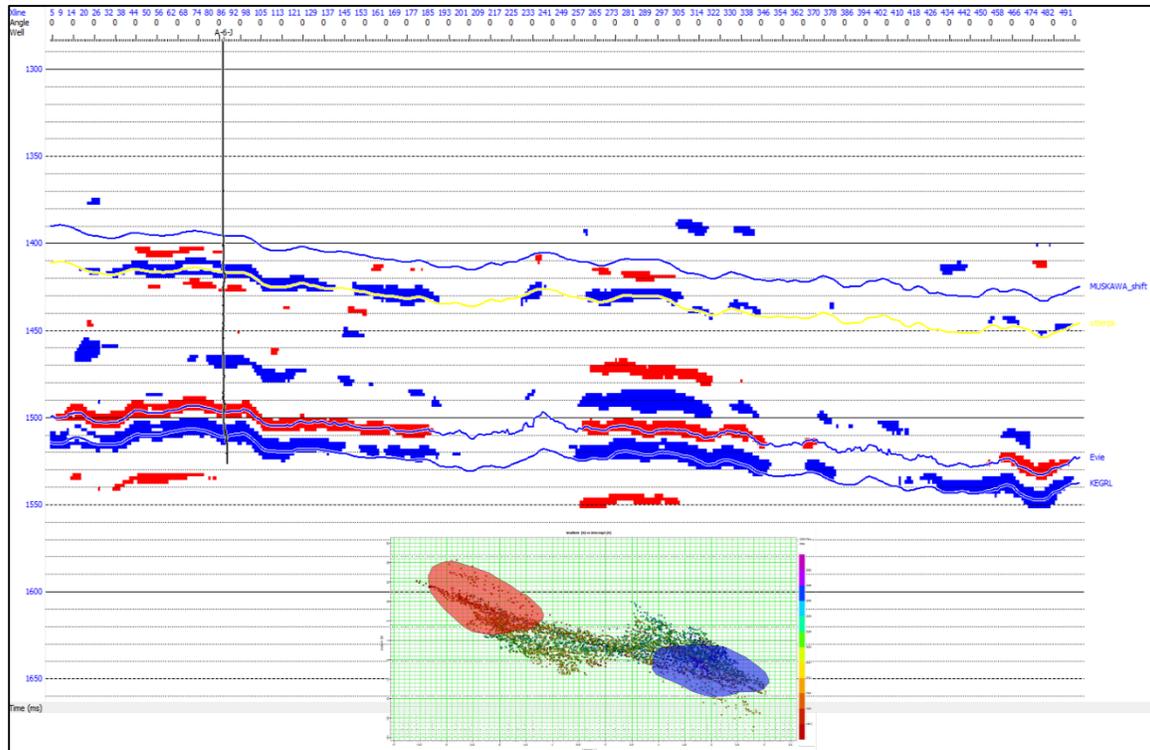
Fig. 21. AVO cross section. Negative intercept and positive gradient is indicated by red. It represents top of class IV reservoir. Blue repents the bottom of the reservoir.

CONCLUSIONS AND FUTURE WORK

For the development of the shale gas reservoir at the Horn River, standard geophysical techniques can be very useful. In this study, we found that post-stack P-impedance inversion can indicate sweet spots. Also, post-stack amplitude, instantaneous frequency, and curvature attributes are useful for identifying fracture direction and intensity. Results of amplitude and instantaneous frequency correlate very well. AVO analysis was found to help identifying top and base of Evie gas away from the well.

We have just received the data in September 2014. Beside standard techniques, we are planning to preform azimuthal analysis for fracture characterization. Our analysis will include AVAZ and VVAZ.

ACKNOWLEDGMENT

workshop and for useful discussion. Also, he would like to thank Nassir Saied for helpful tips in Hampson-Russell software and Dr. Helen Isaac for help with Geoscout software. Finally, he would like to thank Saudi Aramco for graduate study sponsorship.

REFERENCES

Advanced Resources International, 2013, available from: http://www.eia.gov/analysis/studies/worldshalegas/pdf/chaptersi_iii.pdf

Aki, K., and Richards, P.G., 2002, "Quantitative Seismology", 2nd Edition: W.H. Freeman and Company.

CGGVeritas, 2014, Hamson-Rusell Software Manual: Release 9.

Adams, C., 2014, Ministry of Natural Gas Development: Northeast BC Activity Update

Ross, D. J., & Bustin, R. M., 2008, Characterizing the shale gas resource potential of Devonian–Mississippian strata in the Western Canada sedimentary basin: Application of an integrated formation evaluation. AAPG bulletin, 92(1), 87-125.

Rüger, A., 2001, Reflection coefficients and azimuthal AVO analysis in anisotropic media. Society of Exploration Geophysicists.

Roberts, A., 2001, "Curvature attributes and their application to 3D interpreted horizons", First Break, Vol 19.2 February, p. 85-100.

Taner, M. T., Koehler, F., & Sheriff, R. E., 1979, Complex seismic trace analysis. Geophysics, 44(6), 1041-1063.

Thomsen, L., 1986, Weak elastic anisotropy. Geophysics, 51, 1954–1966.